Applied Catalysis B: Environment and Energy 355 (2024) 124195

Contents lists available at ScienceDirect

Applied Catalysis B: Environment and Energy

journal homepage: www.elsevier.com/locate/apcatb

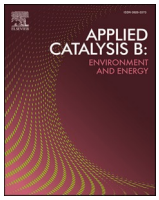

High-temperature shock-resistant zeolite-confined Ru subnanometric species boosts highly catalytic oxidation of dichloromethane

Yanfei Zheng [a,b], Rui Han [a,b], Yunchong Wang [a,b], Weinuo Xu [a,b], Qingling Liu [a,b,*]

[a] Tianjin Key Lab of Indoor Air Environmental Quality Control, School of Environmental Science and Technology, Tianjin University, Tianjin 300350, China
[b] State Key Laboratory of Engines, Tianjin University, Tianjin 300350, China

ARTICLE INFO

Keywords:
Electronic structure
Acid site
Zeolite
Confinement
Stability

ABSTRACT

It is a great challenge to stabilize metal species and regulate their catalytic properties at the atomic level. Herein, we reported the Ru subnanometric species encapsulated inside 5-membered rings of ZSM-5 (Ru@Z-2Al). It achieved 90% oxidation of dichloromethane at 350 °C with almost no by-product formation compared with Ru@Z-0Al. The results indicated that the Al sites existed in the zeolite skeleton provided Brønsted acid sites, which promoted the adsorption and activation of dichloromethane and the extraction of chlorine species. Meanwhile, the electronic structure of Ru species was regulated by Ru−O−Al site, enhancing the oxygen activation capacity of the catalyst and the deep oxidation of dichloromethane. Notably, the Ru@Z-2Al remained stable in harsh environments (at 800 ℃ with 10 vol.% H_2O) due to the double confinement effect of zeolite channels and skeleton Al, which had excellent practical application prospects. Therefore, this study provides insights for designing the high-performance environmental catalytic materials.

1. Introduction

Chlorinated volatile organic compounds (CVOCs) with persistent toxicity and low biodegradability pose a serious threat to the environmental quality and human health. Catalytic oxidation has been recognized as one of the most promising technologies for CVOCs degradation due to its high efficiency and less secondary pollution [1–3]. Supported noble metal catalysts (such as Pt, Pd, Ru, etc.) have been widely studied due to the unfilled d electron orbital, which produces strong adsorption and activation capacity of reactants [4–7]. Given the high price and uneven dispersion of precious metals, researchers have done a lot of work to improve the dispersion of metals [8–10]. However, when the metal active sites are dispersed in the subnanoclusters or even single atoms, the surface free energy of the metals increases, leading to a spontaneous tendency to agglomerate [11,12]. In addition, the sundden high temperature (> 500 ℃) of the reaction-bed in practice also forces the sintering of precious metals and accelerates the deactivation of catalysts [13–15].

Zeolite-encased metals have significant advantages in size control, site adjustment and high-temperature resistance [16–19]. In particular, silicalite-1 (S-1) encased catalysts have been widely studied in the fields of environment and energy fields. For example, Yu et al. prepared well-dispersed ultra-small Pd clusters in S-1 by hydrothermal method, which presented the excellent activity for the complete decomposition of formic acid and high efficiency for hydrogen production under mild conditions [20]. Corma et al. realized the precise localization of highly stable subnanometer Pt and PtSn clusters in S-1, and found that these catalysts showed high stability, selectivity and activity in the dehydrogenation of propane dehydrogenation to propylene [15]. Similarly, Peng et al. designed Rh-Mn bimetallic nanoclusters (1.6 nm) confined in S-1 (Rh-MnOx@S-1). Due to shell confinement and strong metal-metal oxide interaction, Rh-MnOx@S-1 could convert 90% of propane only 264 ℃ [21]. Nevertheless, considering the relatively onefold structure and physicochemical properties of S-1, it is difficult to provide specific active sites for catalytic oxidation of CVOCs. Because the C−Cl bond can often be broken at acidic sites, this will provide an opportunity for subsequent deep oxidation processes. And the introduction of acid sites cannot sacrifice redox sites, otherwise it will lead to the formation of chlorine byproducts [22,23]. Therefore, a reasonable trade-off between acidic and redox sites remains a challenge.

The regulation of the Si-Al ratio has been proven to be an essential factor affecting the acidity of zeilites. This characteristic prompted us to

* Corresponding author at: Tianjin Key Lab of Indoor Air Environmental Quality Control, School of Environmental Science and Technology, Tianjin University, Tianjin 300350, China.
E-mail address: liuql@tju.edu.cn (Q. Liu).

https://doi.org/10.1016/j.apcatb.2024.124195
Received 9 April 2024; Received in revised form 8 May 2024; Accepted 10 May 2024
Available online 13 May 2024

consider whether acid site optimization could be achieved by simply adjusting the Si-Al ratio in metal@zeolite to improve catalyst performance. Here, we obtained a series of Ru@ZSM-5 (Ru@Z) catalysts by using ligand-assisted method, and the Si-Al ratio was adjusted by controlling different Al contents. The successful encapsulation of metal species provides a platform for the close coupling of metal and acid sites in zeolite cavities, which would endow the catalyst excellent activity, product selectivity and high temperature stability in dichloromethane removal. In addition, the effect of the change of Si-Al ratio on the structure and property of the prepared catalyst has also been systematically investigated. Importantly, this work elucidates whether and how Al species interacts with Ru species, which will have important implications for guiding the design of high-performance catalysts.

2. Experimental section

2.1. Chemicals and materials

All chemicals used in this work were analytical grade without further purification, and the details was listed in supporting information. Our previous and Sun et al.'s works were referred to prepare the Ru@Z based catalysts [24–26].

2.2. Synthesis of Ru@Z based catalysts

The 2.6 mL of $RuCl_3$ aqueous solution (1 g/50 mL) was added to the stirred EDA (6.05 g) drop by drop to obtain the Ru-EDA solution. The 8.14 g of TPAOH solution and 18.50 g of deionized water were mixed and stirred for 15 min at room temperature, the X g of aluminium isopropoxide was added (X = 0, 0.01, 0.05, 0.10). Then, the Ru-EDA solution was added and stirred. After that, 8.32 g of TEOS was added drop by drop and stirred continuously 12 h. The resulting solution was then transferred into a 100 mL Teflon-lined stainless-steel autoclave for crystallization (170 ℃, 72 h). After cooling, the product was centrifugally washed with deionized water and dried (100 ℃, 12 h). Finally, the catalysts with different aluminium content named as Ru@Z-0Al, Ru@Z-1Al, Ru@Z-2Al and Ru@Z-3Al were obtained by calcining at 550 ℃ for 4 h. In addition, the synthesis process of ZSM-5 was the same as that of

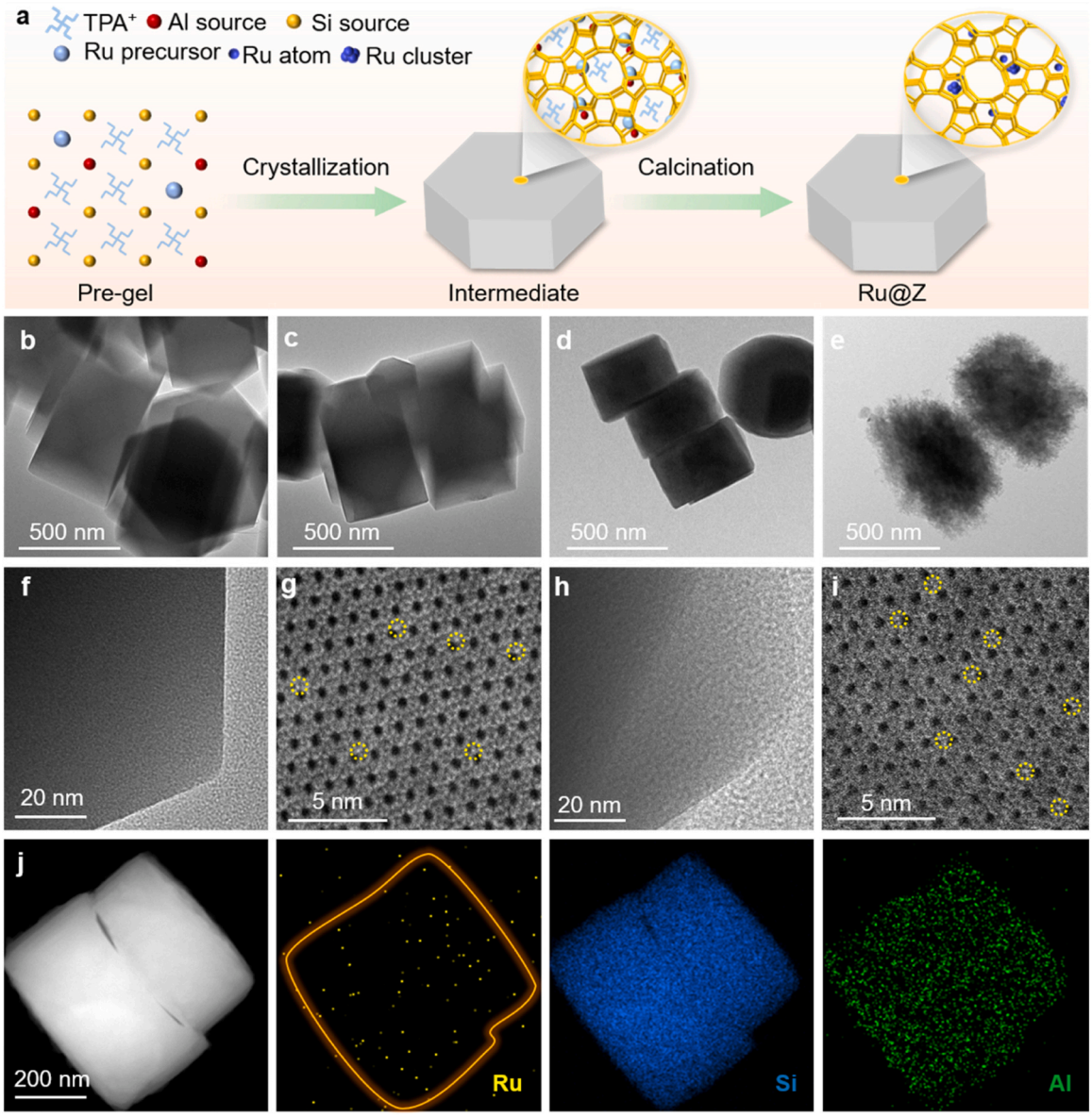

Fig. 1. (a) Illustration of the synthesis process of Ru@Z by hydrothermal method. (b-e) TEM images of Ru@Z-0Al, Ru@Z-1Al, Ru@Z-2Al, Ru@Z-3Al. HRTEM and AC HAADF-STEM images viewed along [010] orientation: (f-g) Ru@Z-0Al. (h-i) Ru@Z-2Al. (j) EDX mapping images of Ru@Z-2Al.

Ru@Z without Ru-EDA precursor solution. For comparison, the Ru/Z-2Al catalyst supported with Ru on zeolite (Ru/Z) was prepared by impregnation method. Specifically, a certain amount of $RuCl_3$ aqueous solution (1 g/50 mL) was added to 1 g of ZSM-5, stationary for 12 h, and then it was dried and calcined.

2.3. Catalyst activity measurement and characterizations

The catalytic oxidation test of DCM was carried out in a fix-bed quartz tube (8 mm i.d. × 400 mm length), and 0.10 g of sample was placed. In the reaction, 1000 ppm of DCM, 21 vol% of O_2, and balanced N_2 were introduced into the fixed bed with a 25 mL/min flow rate. The gas hourly space velocity of the reaction was 15, 000 mL/(g·h). The concentration of DCM was measured by gas chromatograph (GC-9790, FuLi) with two FID detectors [27]. The detailed characterization procedures were described in supporting information.

3. Results and discussion

3.1. Preparation and characterizations of catalysts

Fig. 1a exhibits the in situ hydrothermal synthesis of ultrafine Ru species encapsulated in zeolite (named Ru@Z). According to Yu et al. and Iglesia et al., the ethylenediamine ligand-assisted method can inhibit the rapid precipitation of metals in a strong alkali environment [28,29]. Here we learned from the above method, adding a certain amount of metal precursor to the pre-gel of synthetic zeolite to ensure the successful encapsulation of metal. It is worth noting that the different contents of aluminium isopropoxide were introduced in the synthesis process, and a series of Ru@Z catalysts with different Si/Al ratios were finally obtained. Table S2 lists the aluminum content and Si-Al ratio of the catalyst. The Ru@Z-1Al, Ru@Z-2Al and Ru@Z-3Al with Al content of 0.13, 0.44 and 0.71 wt% correspond to Si/Al ratios of

142, 77 and 57, respectively. The content of Ru measured by ICP-AES is ~0.3 wt% in Ru@Z-0Al, Ru@Z-1Al and Ru@Z-2Al, while only 0.19 wt% of Ru in Ru@Z-3Al. This indicates that adding too much Al would lead to a decrease in the amount of Ru (Table S2). Compared with ZSM-5, the results of N_2 adsorption-desorption show that the pore volume of the samples is reduced from 0.32 cm^3/g to 0.22 cm^3/g, which possibly because the occupation of Ru species [30]. The XRD patterns in Fig. S1 shows that the samples exhibit a typical MFI crystal structure (JCPDS no. 49-0657) and the Ru-related species have not been observed [31,32]. It is worth noting that the crystallinity gradually decreases with the increase of the Al content. The TEM images show a consistent phenomenon. The Ru@Z-0Al (Fig. 1b) shows hexahedral shape, and with the addition of Al, the morphology does not change significantly although the crystal size is slightly reduced (Fig. 1c, d). Meanwhile, no Ru species were observed on either the surface or the edge of the catalyst (Fig. 1 f, h and Fig. S4), which may be due to the ultrafine Ru species (clusters or single-atom) encapsulated in zeolite. However, if the Al content is too high, such as Ru@Z-3Al, the zeolite structure collapses and exposes larger Ru nanoparticles with 10.5 nm exposed (Fig. 1e and Fig. S5, S6). The AC HAADF-STEM images of the Ru@Z-0Al and Ru@Z-2Al further confirm that the Ru species is confined within ZSM-5. It can be observed that the 10-membered rings (MRs) channel is empty (Fig. 1g, i), and the brighter signals can be inferred that Ru species are highly distributed as atoms or clusters around the 5-MRs of ZSM-5 (Fig. S7) [28].

XPS was used to investigate the location of Ru species. As we can see, no Ru signal is observed in Ru@Z-0Al, Ru@Z-1Al and Ru@Z-2Al (Fig. S8a–c), indicating that the Ru species were successfully encapsulated into zeolite [33,34]. However, a distinct Ru signal was detected on the surface of Ru@Z-3Al (Fig. S8d). These results demonstrate that the successful encapsulation of Ru species with the appropriate Al

content introduction. However, the excessive introduction of Al leads to the decrease of the crystallinity and the structural collapse of the zeolite, and the confinement effect on Ru species is weakened, which is also consistent with TEM results (Fig. 1e) [35–37]. To investigate the valence state and electronic structure of the catalysts, the XPS signal of the Ru 3p was obtained by Ar^+ ion sputtering for 100 s. As shown in Fig. 2a, with the addition of Al, the binding energy of Ru 3p gradually moves to the higher, indicating that the electron density around Ru decreases. Moreover, the binding energy of Al 2p moves towards the lower, indicating that the electron density of Al increases (Fig. S9). This may be due to the interaction of Ru species with the Al site of zeolite [38]. This phenomenon was further verified by the X-ray absorption fine structure (XAFS). The X-ray absorption near edge structure (XANES) of Ru K-edge spectra was displayed in Fig. 2b. The K-edge position of Ru species in Ru@Z-0Al and Ru@Z-2Al shifts toward higher energies compared to Ru foil, which demonstrates that the Ru species in the samples have a higher average oxidation state than in the Ru foil [39]. This result verifies that the more Ru species coordinates with oxygen atoms to form isolated Ru atoms or RuO_x clusters [28,40]. Notely, the white-line intensity of Ru@Z-2Al slightly raises compared to Ru@Z-0Al, suggesting the higher valence state of Ru species in Ru@Z-2Al. This may be due to the formation of more Ru−O−M bonds between Ru and the zeolite support [41,42]. The Ru species were further studied by EXAFS spectra in R space. Fig. 2c and Fig. S10 show that the Ru−Ru bond and weak Ru−O bond are identified in Ru@Z-0Al, implying that the Ru clusters are dominant. After the introduction of Al, however, the Ru−O bond is stronger in Ru@Z-2Al (Fig. 2f), which may be due to the formation of more Ru−O−Al sites stabilized by the Al sites of the zeolite skeleton [43–45]. This site plays a key role in avoiding aggregation of Ru species in harsh environments. These result indicates that the electronic structure of Ru changed after the Al adding, which is consistent with the XPS results.

The ^{27}Al MAS NMR was employed to elucidate the location of introduced Al. As depicted in Fig. 2g, the spectra shows that Al in ZSM-5 exists in tetrahedral framework aluminum (FAL) species and octahedral extraframework aluminum (EFAL) species [46]. Notably, after Ru encapsulation, the Ru@Z-1Al and Ru@Z-2Al contain almost only FAL species (99%) (Fig. 2h), mainly from the interaction between FAL and neighboring Ru species [30]. This is also consistent with the results of XPS and XAFS. Previous studies have confirmed that frame Al atoms in zeolite correspond to Brønsted acid sites (B acid) [36]. NH_3-TPD and Pyridine FT-IR tests were employed to study the acidity strength and types. NH_3-TPD results in Fig. S11 show a higher total acid content in Ru@Z-2Al, which is beneficial for DCM adsorption [47]. As shown in the embedded picture in Fig. 2i, the bands 1445, 1491 and 1545 cm^{-1} are attributed to Lewis acid (L acid), B and L acid, and B acid, respectively [48]. The ratio of B acid to L acid was calculated and shown in Fig. 2i. As we expected, the B/L acid ratio increased with the increase of Al, which favors chlorine removal and HCl generation [49,50].

3.2. Activity and stability tests of Ru@Z catalysts for dichloromethane oxidation

Dichloromethane (DCM) as a typical hard-to-degrade chlorinated volatile organic

compound (CVOC), has a wide range of industrial sources, such as synthetic resin, printing, pharmaceutical, pesticide manufacturing, electronics manufacturing, etc., which seriously impact human health and atmospheric environment [1,4,51]. Therefore, DCM was chosen as the research object here. Fig. 3a exhibits the conversion efficiency of various samples for DCM. Compared with the non-Al zeolite (S-1) that only converts 20% DCM at 350 ℃, the ZSM-5 with Al has a higher conversion efficiency, corresponding to 75% conversion at 350 ℃. However, the CO_2 yield of ZSM-5 is close to that of S-1, as low as 10% (Fig. 3b). It is worth noting that the complete oxidation of CVOC without byproducts is more important than the conversion rate, because the chlorination byproducts are prone to produce more toxic substances such as polychlorobenzene and dioxins [52–54]. As one of the typical

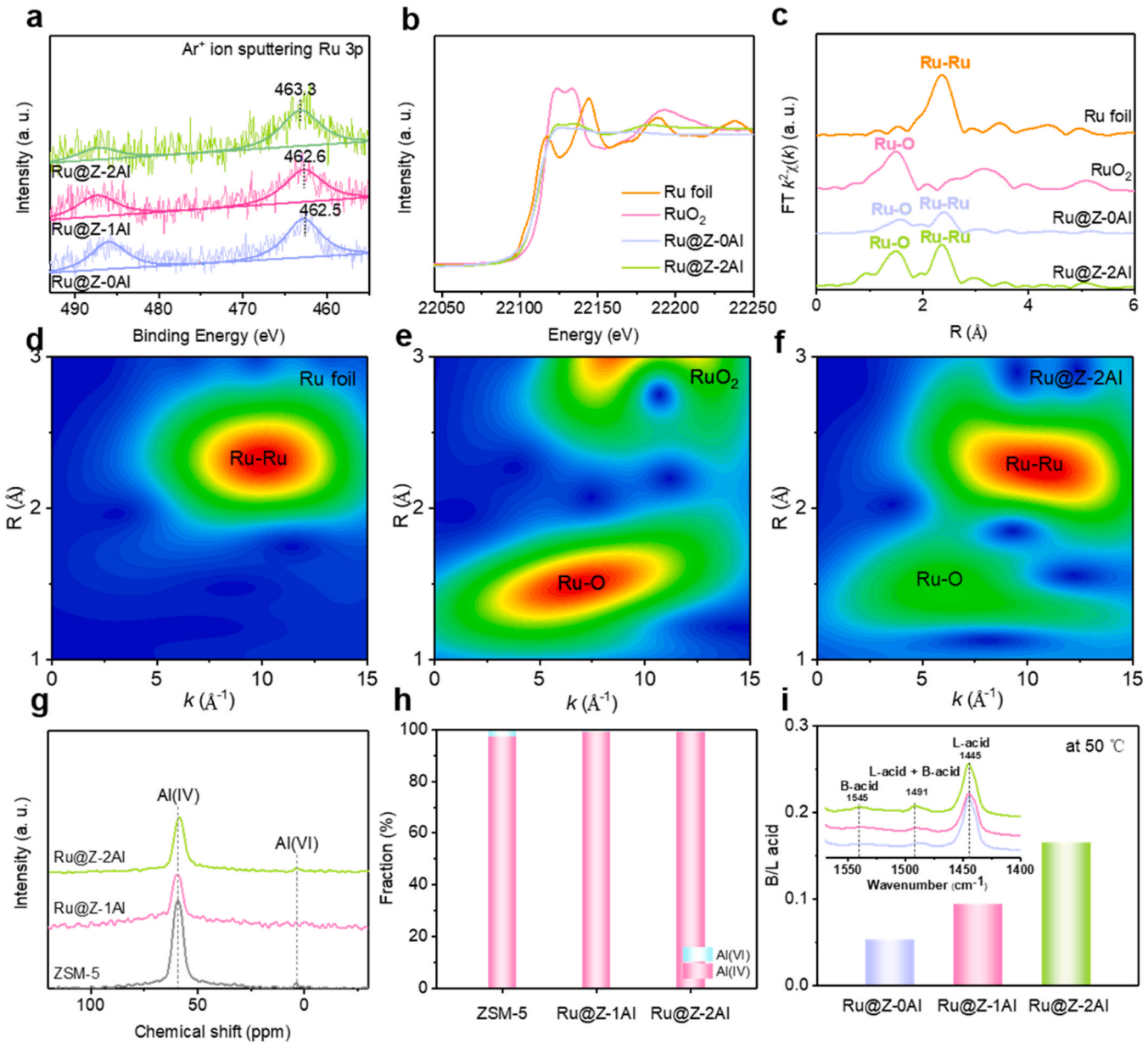

Fig. 2. (a) Ru 3p XPS. (b) The Ru K-edge XANES profiles. (c) Fourier transforms of k^2-weighted Ru K-edge of EXAFS spectra. WT k^2-weighted EXAFS spectra: (d) Ru foil. (e) RuO_2. (f) Ru@Z-2Al. (g) ^{27}Al MAS NMR spectra. (h) The proportion of aluminum species in different locations. (i) The ratio of B/L acid by Pyridine FT-IR results.

by-products, chloromethane is produced in large quantities on ZSM-5, indicating that the ZSM-5 plays a decisive role in breaking the C−Cl bond in DCM (Fig. 3c). Nevertheless, its deep oxidation capacity is limited due to the lack of redox active sites (Fig. 3d).

Further, we introduced Ru species as redox sites and studied the effect of different Al content on catalyst performance. As depicted in Fig. 4a, it can be seen that with the increase of Al content, DCM degradation efficiency gradually increases until Ru@Z-3Al, which may be due to the low Ru content and weak confinement effect of Ru@Z-3Al. The reaction rate of the catalysts with temperature was calculated in Fig. S12a and the value at 350 ℃ (DCM conversion rate of 90%) was depicted in Fig. 4b. It is not difficult to find that the Ru@Z-2Al has the most significant reaction rate (1.1×10^{-7} mol/g·s). In addition, the apparent activation energy is also consistent with the activity trend in Fig. 4c, that is, Ru@Z-2Al (23.3 kJ/mol) < Ru@Z-3Al (23.5 kJ/mol) < Ru@Z-1Al (26.6 kJ/mol) < Ru@Z-0Al (30.8 kJ/mol). It is essential that almost no chlorine-containing byproducts were produced on Ru@Z-2Al (Fig. S12b, c and Fig. S24), which has a high CO_2 yield compared with literature reports (Table S3). In addition, the effect of confinement effect on catalytic activity was investigated by testing the performance of the Ru-supported Ru/Z-2Al catalyst (Ru/Z). It is found that although it has a high degradation activity of DCM, it is accompanied by incomplete degradation of chloromethane (Fig. 3c). Besides, the Ru/Z catalyst did not perform well in the face of sudden high-temperature environments (Fig. S13a–c). It is further confirmed that the confinement effect of zeolite provides an opportunity to enhance activity and stability.

Considering that the temperature of the reaction bed would suddenly rise (≥500 ℃), the high-temperature tolerance of the catalysts was tested. It is exciting that the Ru@Z-2Al catalyst shows excellent stability under the intermittent high-temperature impact at 500, 600, 700, or 800 ℃ (Fig. S13d and Fig. 4d–f). However, the DCM degradation and CO_2 yield of Ru@Z-0Al decreased significantly after high temperature impact (Fig. 4d, e). The yield of chloromethane increased gradually (Fig. 4f). This shows that the presence of Al species is essential for the

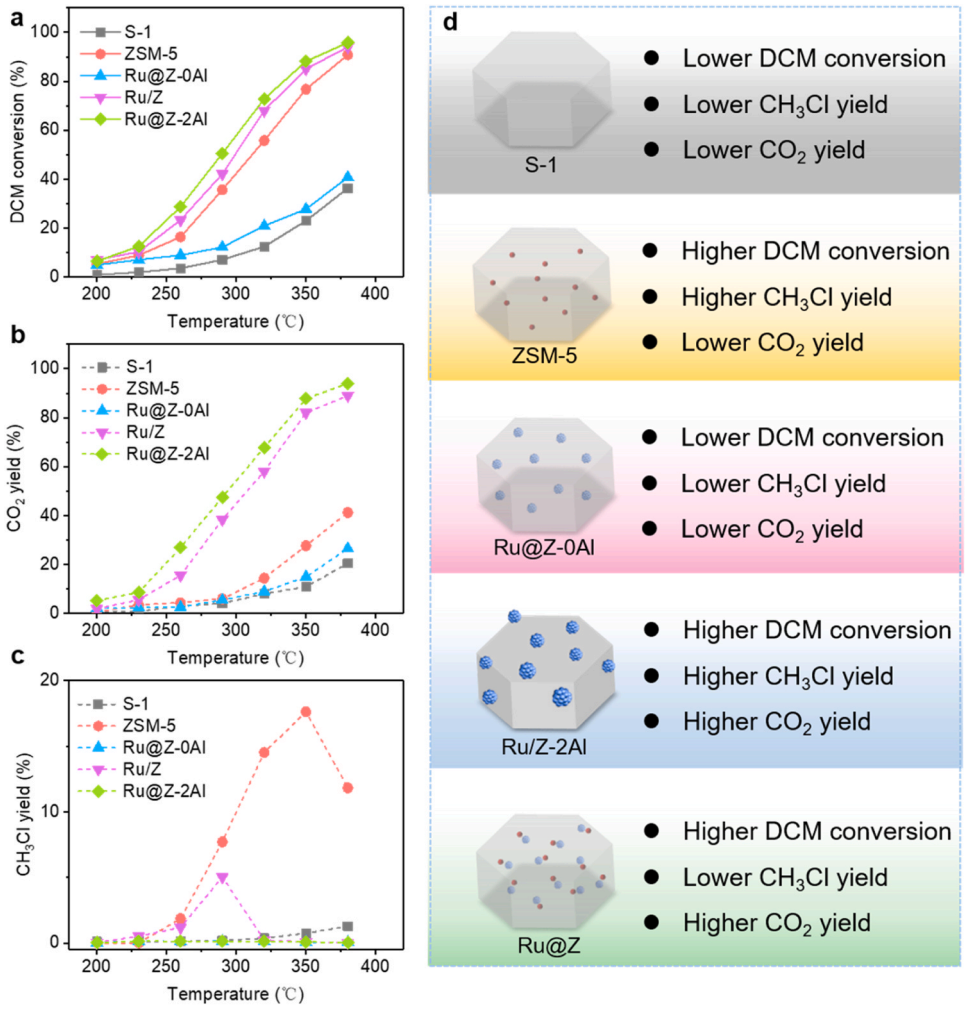

Fig. 3. (a) DCM conversion. (b) CO_2 yield. (c) CH_3Cl yield. (d) Performance comparison on S-1, ZSM-5, Ru@Z-0Al, Ru@Z-2Al and Ru/Z-2Al (Ru/Z).

catalyst to calm in the face of sudden high-temperature impact. In addition, water vapor is also usually present in the exhaust gas, the catalytic property of Ru@Z-2Al and Ru@Z-0Al in the presence of water vapor has been tested. As depicted in Fig. S14, the activity of the two catalysts are almost not affected by water vapor. Further, the tests in DCM oxidation with 10 vol.% H_2O at 800 ℃ for 10 h were performed to investigate the stability. As shown in Fig. 4g–i, the DCM conversion, CO_2 yield, and CH_3Cl yield on the Ru@Z-2Al were not affected, indicating that the ability of the catalyst to destroy the C−Cl bond and deep oxidation was well preserved. The results of HAADF-STEM images and XRD of Ru@Z-2Al after hydrothermal treatment (Fig. S15-16) show that the Ru species is still highly dispersed rather than aggregated. On the Ru@Z-0Al without Al, the DCM conversion is slightly increased, possibly due to the water molecules providing H protons, promoting DCM adsorption and dissociation. However, due to the high temperature, the Ru clusters are agglomerate to 4.3 nm (Fig. S17), thus weakening the deep oxidation capacity and resulting in a large amount of chloromethane. The above results further confirm that the Al site in zeolite skeleton plays a key role in anchoring and stabilizing metal cations.

Fig. 4j shows that the Ru@Z-2Al can stabily react at 350 ℃ for at least 130 h. And, no signal of Cl 2p was detected by XPS and EDS mapping, indicating that no chlorine species were deposited on the catalyst (Fig. S18). Fig. 4k shows a slight decrease in DCM conversion after 5 or 10 vol.% H_2O, possibly due to competitive adsorption between water vapor and DCM. Fig. S19 shows that the Ru@Z-2Al has good recycling ability. The above test results show that Ru@Z-2Al not only has high activity but also has excellent stability, giving it great potential for industrial application.

3.3. *Verifying the origination of catalytic performance*

Considering the difference between Ru@Z-3Al and other samples in crystallinity and metal content, we will focus on several other catalysts (Ru@Z-0Al, Ru@Z-1Al, Ru@Z-2Al) below to better elucidate the relationship between the structure and performance. DCM-TPD (Fig. 5a) and in situ DRIFTS spectra of DCM adsorption (Fig. 5b and Fig. S20) experiments further confirm that the catalyst has stronger adsorption capacity for DCM after adding Al. The redox property of catalysts is another critical factor that affects their catalytic performance. In Fig. 5c, the H_2-TPR result shows that the reduction peak at ~160 ℃ is attributed to the RuOx species [50,55]. It is worth noting that new reduction peaks at 307 and 382 ℃ in the Ru@Z-2Al indicate a novel interaction caused by the Ru−O−Al site, consistent with results of XPS and XAFS [56]. Oxygen species below 200 ℃ and 300–400 ℃ belong to surface adsorbed oxygen and lattice oxygen species, respectively (Fig. S21) [27]. With the introduction of

Al, the surface oxygen species increased significantly, promoting the deep oxidation of DCM. To better demonstrate the activation ability of oxygen species in the catalyst, the products in the DCM-TPD tests were compared (Fig. S22). Fig. 5d shows that a signal of HCl is detected at 100 ℃ and the HCl production increases as Al content increases, which correlates with higher B acids in the catalyst [47]. With the temperature increasing, H_2O and CO_2 are generated on the catalysts. It is noteworthy that Ru@Z-2Al produces the highest amount of the content of H_2O and

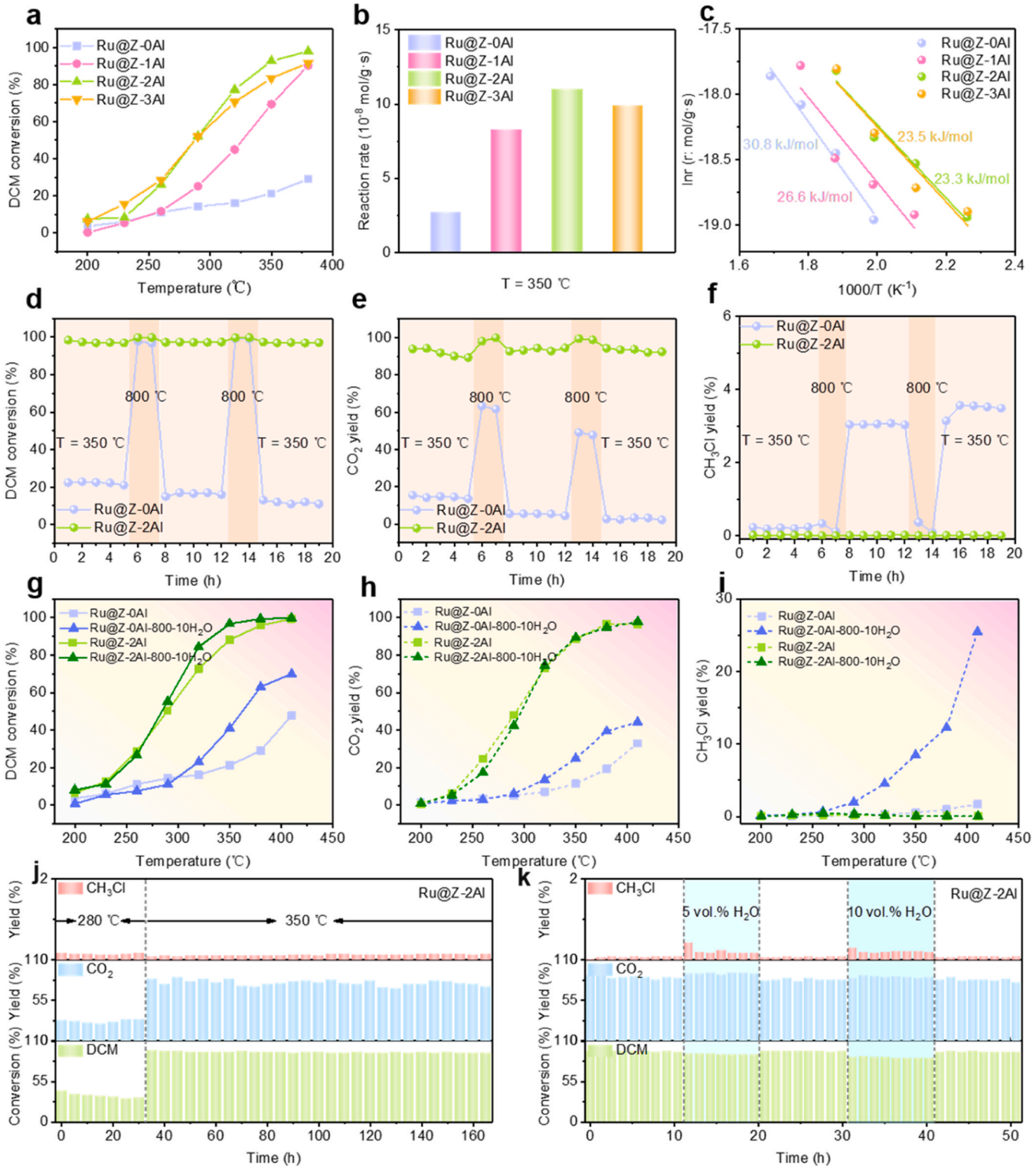

Fig. 4. (a) DCM conversion. (b) Reaction rate at 350 ℃. (c) Arrhenius plots of Ru@Z-0Al, Ru@Z-1Al, Ru@Z-2Al and Ru@Z-3Al. stability test of high temperature shock on Ru@Z-2Al and Ru@Z-0Al for DCM oxidation: (d) DCM conversion. (e) CO_2 yield. (f) CH_3Cl yield. Comparison of activity before and after treatment at 800 ℃ with 10 vol.% H_2O: (g) DCM conversion. (h) CO_2 yield. (i) CH_3Cl yield. (j) Long-term stability of Ru@Z-2Al at 280 and 350 ℃. (k) Stability of Ru@Z-2Al in the present of water vapor at 350 ℃.

CO_2 (Fig. 5e, f), due to the more content reactive oxygen species involved in the reaction.

Then, the catalysts were pretreated with oxygen gas, and the products of the DCM reaction process without oxygen gas were collected to study the activation ability of the catalyst to oxygen gas. As shown in Fig. S23, compared with the Ru@Z-0Al without Al, the chloromethane and HCl are more easily formed on Ru@Z-2Al (Fig. S20b), suggesting that it is more likely to promote C–Cl bond breaking and facilitate subsequent deep oxidation. In addition, H_2O and CO_2 are easily formed on the Ru@Z-2Al, and their production temperature is consistent with

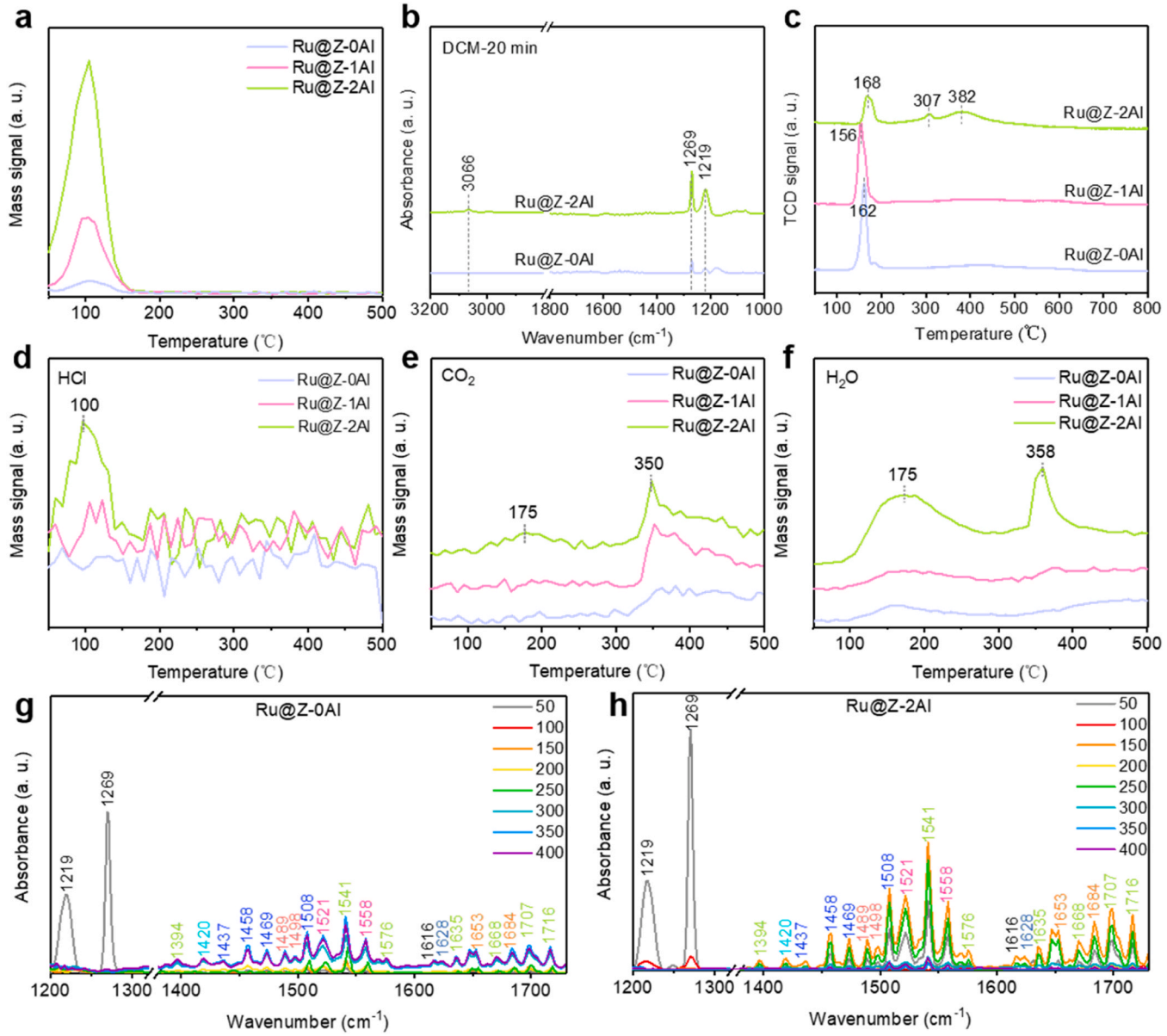

Fig. 5. (a) DCM-TPD curve. (b) in situ DRIFTS spectra of DCM adsorption. (c) H_2-TPR curve. The products in DCM-TPD tests: (d) HCl signal. (e) CO_2 signal. (f) H_2O signal. In situ DRIFTS spectra of DCM oxidation: (g) Ru@Z-0Al. (h) Ru@Z-2Al.

the desorption temperature of surface adsorbed oxygen and lattice oxygen. Therefore, the interaction of Ru and Al enhances the oxygen activation capacity of the catalyst. In addition, the products of the reaction were further detected by mass spectrometry (Fig. S24). With the increase of Al content, the formation temperature of the main product, such as CO_2, H_2O, and HCl (Fig. S25) shifted to a lower temperature. At the same time, the formation of chlorine byproducts and CO are significantly inhibited. However, due to the lack of acidic sites, polychlorinated by-products such as $CHCl_3$ and CCl_4 were detected on the surface of Ru@Z-0Al (Fig. S26c–d). Based on the above analysis, the introduction of skeleton Al affects the activity in two ways: (i) affecting the acidity of the catalyst, which in turn affects the adsorption and activation ability of the catalyst for DCM; (ii) regulating the electronic structure of Ru species, further affects the deep oxidation performance of DCM.

The detailed reaction pathway was explored by in situ DRIFTS experiments on Ru@Z-0Al and Ru@Z-2Al. Fig. 5g, h show that the adsorption bands (1219, 1269 and 1616 cm^{-1}) attributing to gaseous DCM decrease with increasing temperature and completely disappear at 100 ℃ [57]. It is worth noting that the DCM signal (1269 cm^{-1}) of the Ru@Z-2Al is stronger than Ru@Z-0Al, further confirming that DCM is more easily adsorbed on the catalyst. As the temperature rises, many new bands appear. The band at 1394 cm^{-1} is ascribed to the C–H displacement of formate species [58]. The bands at 1437, 1469 and 1558 cm^{-1} are attributed to C–H bending vibrations of chloromethoxy (CH_2ClO–) species, resulting from the first dehydrochlorination between DCM and catalyst [59–61]. The band at 1423 cm^{-1} is attributed to bidentate methoxy species (–OHCHO–), produced through the second nucleophilic substitution [59]. The bands at 1489 and 1498 cm^{-1} are attributed to CH_2 vibrations of formaldehyde (CH_2O–), which could be due to the methoxy species reacting with H_2O [62,63]. The band at 1628 cm^{-1} is attributed to the adsorbed H_2O [64]. In addition, a large number of bands that assigned to v(COO) of formate species were observed, such as the bands at 1521, 1541, 1558, 1578, 1635, 1655, 1668, 1707, 1716 cm^{-1} [59,63,65–68], indicating that dechlorination and further oxidation processes at a lower temperature are more likely to occur on the Ru@Z-2Al catalyst. Therefore, the possible reaction process of DCM on Ru@Z-2Al is as follows (Fig. 6). Firstly, the DCM

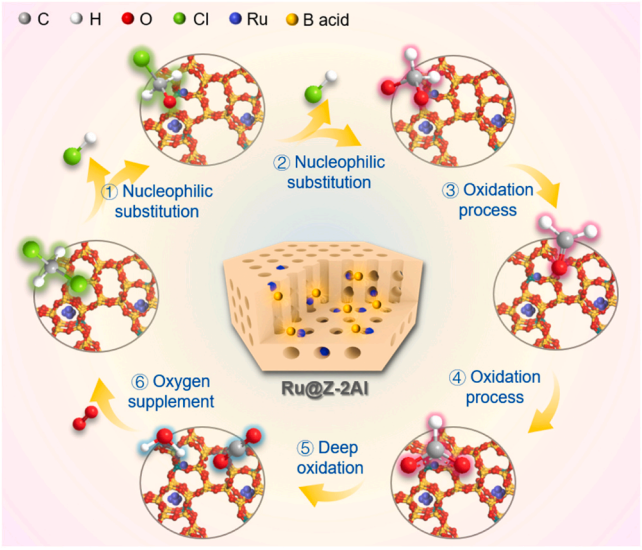

Fig. 6. Proposed pathways of DCM oxidation over the Ru@Z-2Al.

adsorbed and activated at the acid site, which accelerates the extraction of chlorine and produces HCl due to the presence of the B acid site. Then, the intermediate species (chloromethoxy, bidentate methoxy and formate species) undergo deep oxidation on the Ru species with higher oxidation state, ultimately producing CO_2 and H_2O. Due to the confinement effect of zeolite, the Ru@Z-2Al overcomes the problem that the intermediate product cannot be oxidized rapidly due to the large distance between the B acid site and the precious metal site. Importantly, due to the stabilizing effect of Al on Ru species by Ru−O−Al site, the catalyst is calm to the harsh environment. (Fig. 4d–i and Fig. S13d).

4. Conclusions

In summary, we have successfully confined the Ru subnanometric species to the 5-MR channel of structurally stable ZSM-5, and achived high efficiency oxidation of dichloromethane through simple Si-Al ratio regulation. This highly dispersed Ru species was formed under the synergistic confinement of the skeleton Al and zeolite pores. A series of characterizations analyses have identified the roles played by Al species. It not only introduces the B acid site to rise the adsorption of DCM, but also effectively regulates the electronic structure of Ru species to enhance the oxidation ability of catalyst for DCM. It is satisfactory that the Ru@Z-2Al catalyst produces almost no chlorine-containing byproducts and can stabilize the reaction in harsh environments. Thus, this work provides the preparation method of a stable and high-performance catalysts, and it is also expected to influence the understanding of zeolite-encaged metal active species.

CRediT authorship contribution statement

Qingling Liu: Writing – review & editing. **Weinuo Xu:** Conceptualization. **Yunchong Wang:** Conceptualization. **Rui Han:** Supervision. **Yanfei Zheng:** Writing – original draft.

Declaration of Competing Interest

The authors declare that they have no known competing financial interests or personal relationships that could have appeared to influence the work reported in this paper.

Data Availability

Data will be made available on request.

Acknowledgements

The work was supported by the National Natural Science Foundation of China (Nos. 22276133, U20A20132 and 52106180), the National Key R&D Program of China (2022YFB3504100, 2022YFB3504102, 2019YFC1903900 and 2019YFC1903902).

Appendix A. Supporting information

Supplementary data associated with this article can be found in the online version at doi:10.1016/j.apcatb.2024.124195.

References

[1] Y. Su, K. Fu, C. Pang, Y. Zheng, C. Song, N. Ji, D. Ma, X. Lu, C. Liu, R. Han, Q. Liu, Recent advances of chlorinated volatile organic compounds' oxidation catalyzed by multiple catalysts: reasonable adjustment of acidity and redox properties, Environ. Sci. Technol. 56 (2022) 9854–9871.
[2] Q. Dai, L.-L. Yin, S. Bai, W. Wang, X. Wang, X.-Q. Gong, G. Lu, Catalytic total oxidation of 1,2-dichloroethane over VOx/CeO_2 catalysts: further insights via isotopic tracer techniques, Appl. Catal. B-Environ. Energy 182 (2016) 598–610.
[3] X. Weng, Q. Meng, J. Liu, W. Jiang, S. Pattisson, Z. Wu, Catalytic oxidation of chlorinated organics over lanthanide perovskites: effects of phosphoric acid etching and water vapor on chlorine desorption behavior, Environ. Sci. Technol. 53 (2019) 884–893.
[4] C. He, J. Cheng, X. Zhang, M. Douthwaite, S. Pattisson, Z. Hao, Recent advances in the catalytic oxidation of volatile organic compounds: a review based on pollutant sorts and sources, Chem. Rev. 119 (2019) 4471–4568.
[5] M.A. Salaev, A.A. Salaeva, T.S. Kharlamova, G.V. Mamontov, $Pt–CeO_2$-based composites in environmental catalysis: a review, Appl. Catal. B-Environ. Energy 295 (2021) 120286.
[6] X. Yang, Q. Li, E. Lu, Z. Wang, X. Gong, Z. Yu, Y. Guo, L. Wang, Y. Guo, W. Zhan, J. Zhang, S. Dai, Taming the stability of Pd active phases through a compartmentalizing strategy toward nanostructured catalyst supports, Nat. Commun. 10 (2019) 1611.
[7] H. Peng, T. Dong, S. Yang, H. Chen, Z. Yang, W. Liu, C. He, P. Wu, J. Tian, Y. Peng, X. Chu, D. Wu, T. An, Y. Wang, S. Dai, Intra-crystalline mesoporous zeolite encapsulation-derived thermally robust metal nanocatalyst in deep oxidation of light alkanes, Nat. Commun. 13 (2022) 295.
[8] Z. Li, S. Ji, Y. Liu, X. Cao, S. Tian, Y. Chen, Z. Niu, Y. Li, Well-defined materials for heterogeneous catalysis: from nanoparticles to isolated single-atom sites, Chem. Rev. 120 (2020) 623–682.
[9] A.J. Therrien, A.J.R. Hensley, M.D. Marcinkowski, R. Zhang, F.R. Lucci, B. Coughlin, A.C. Schilling, J.-S. McEwen, E.C.H. Sykes, An atomic-scale view of single−site Pt catalysis for low−temperature CO oxidation, Nat. Catal. 1 (2018) 192–198.
[10] X. Yang, A. Wang, B. Qiao, J. Li, J. Liu, T. Zhang, Single-atom catalysts: a new frontier in heterogeneous catalysis, Acc. Chem. Res. 46 (2013) 1740–1748.
[11] R. Lang, W. Xi, J.C. Liu, Y.T. Cui, T. Li, A.F. Lee, F. Chen, Y. Chen, L. Li, L. Li, J. Lin, S. Miao, X. Liu, A.Q. Wang, X. Wang, J. Luo, B. Qiao, J. Li, T. Zhang, Non defect-stabilized thermally stable single-atom catalyst, Nat. Commun. 10 (2019) 234.
[12] Y. Ren, Y. Tang, L. Zhang, X. Liu, L. Li, S. Miao, D. Sheng Su, A. Wang, J. Li, T. Zhang, Unraveling the coordination structure-performance relationship in Pt_1/Fe_2O_3 single-atom catalyst, Nat. Commun. 10 (2019) 4500.
[13] A. Aitbekova, C. Zhou, M.L. Stone, J.S. Lezama-Pacheco, A.-C. Yang, A.S. Hoffman, E.D. Goodman, P. Huber, J.F. Stebbins, K.C. Bustillo, P. Ercius, J. Ciston, S.R. Bare, P.N. Plessow, M. Cargnello, Templated encapsulation of platinum-based catalysts promotes high-temperature stability to 1100 °C, Nat. Mater. 21 (2022) 1290–1297.
[14] B. Zhang, L. Zhou, M. Qi, Z. Li, J. Han, K. Li, Y. Zhang, F. Dehghani, R. Liu, J. Yun, outstanding stability and enhanced catalytic activity for toluene oxidation by Si-O-Mn interaction over $MnOx/SiO_2$, Ind. Eng. Chem. Res. 61 (2022) 1044–1055.
[15] L. Liu, M. Lopez−Haro, C.W. Lopes, C. Li, P. Concepcion, L. Simonelli, J.J. Calvino, A. Corma, Regioselective generation and reactivity control of subnanometric platinum clusters in zeolites for high−temperature catalysis, Nat. Mater. 18 (2019) 866–873.
[16] Q. Zhang, S. Gao, J. Yu, Metal sites in zeolites: synthesis, characterization, and catalysis, Chem. Rev. 123 (2022) 6039–6106.
[17] L. Liu, A. Corma, Confining isolated atoms and clusters in crystalline porous materials for catalysis, Nat. Rev. Mater. 6 (2020) 244–263.
[18] H. Wang, L. Wang, F.S. Xiao, Metal@Zeolite hybrid materials for catalysis, ACS Cent. Sci. 6 (2020) 1685–1697.
[19] Y. Chai, W. Shang, W. Li, G. Wu, W. Dai, N. Guan, L. Li, Noble metal particles confined in zeolites: synthesis, characterization, and applications, Adv. Sci. 6 (2019) 1900299.
[20] N. Wang, Q. Sun, R. Bai, X. Li, G. Guo, J. Yu, In situ confinement of ultrasmall Pd clusters within nanosized silicalite-1 zeolite for highly efficient catalysis of hydrogen generation, J. Am. Chem. Soc. 138 (2016) 7484–7487.
[21] W. Liu, J. Tao, Y. Zhao, L. Ren, C. Li, X. Wang, J. Chen, J. Lu, D. Wu, H. Peng, Boosting the deep oxidation of propane over zeolite encapsulated Rh-Mn bimetallic nanoclusters: elucidating the role of confinement and synergy effects, J. Catal. 413 (2022) 201–213.

[22] N. Zhang, Y. Guo, Y. Guo, Q. Dai, L. Wang, S. Dai, W. Zhan, Synchronously constructing the optimal redox−acidity of sulfate and RuO_x Co-modified CeO_2 for catalytic combustion of chlorinated VOCs, Chem. Eng. J. 454 (2023) 140391.

[23] Q. Dai, K. Shen, W. Deng, Y. Cai, J. Yan, J. Wu, L. Guo, R. Liu, X. Wang, W. Zhan, HCl-Tolerant H_xPO_4/RuO_x-CeO_2 catalysts for extremely efficient catalytic elimination of chlorinated VOCs, Environ. Sci. Technol. 55 (2021) 4007–4016.

[24] L. Yang, Q. Liu, R. Han, K. Fu, Y. Su, Y. Zheng, X. Wu, C. Song, N. Ji, X. Lu, D. Ma, Confinement and synergy effect of bimetallic Pt-Mn nanoparticles encapsulated in ZSM-5 zeolite with superior performance for acetone catalytic oxidation, Appl. Catal. B-Environ. Energy 309 (2022) 121224.

[25] Q. Sun, B.W.J. Chen, N. Wang, Q. He, A. Chang, C.M. Yang, H. Asakura, T. Tanaka, M.J. Hulsey, C.H. Wang, J. Yu, N. Yan, Zeolite-encaged Pd-Mn nanocatalysts for CO_2 hydrogenation and formic acid dehydrogenation, Angew. Chem. Int. Ed. 59 (2020) 20183–20191.

[26] Y. Zheng, R. Han, L. Yang, J. Yang, C. Shan, Q. Liu, Revealing opposite behaviors of catalyst for VOCs oxidation: modulating electronic structure of Pt nanoparticles by Mn doping, Chem. Eng. J. 465 (2023) 142807.

[27] Y. Zheng, Y. Su, C. Pang, L. Yang, C. Song, N. Ji, D. Ma, X. Lu, R. Han, Q. Liu, Interface−enhanced oxygen vacancies of CoCuOx catalysts in situ grown on monolithic Cu foam for VOC catalytic oxidation, Environ. Sci. Technol. 56 (2022) 1905–1916.

[28] Q. Sun, N. Wang, T. Zhang, R. Bai, A. Mayoral, P. Zhang, Q. Zhang, O. Terasaki, J. Yu, Zeolite-encaged single-atom rhodium catalysts: highly-efficient hydrogen generation and shape-selective tandem hydrogenation of nitroarenes, Angew. Chem. Int. Ed. *58* (2019) 18570–18576.

[29] T. Otto, S.I. Zones, E. Iglesia, Synthetic strategies for the encapsulation of nanoparticles of Ni, Co, and Fe oxides within crystalline microporous aluminosilicates, Microporous Mesoporous Mater. 270 (2018) 10–23.

[30] J. Yang, Y. He, J. He, Y. Liu, H. Geng, S. Chen, L. Lin, M. Liu, T. Chen, Q. Jiang, B. M. Weckhuysen, W. Luo, Z. Wu, Enhanced catalytic performance through in situ encapsulation of ultrafine Ru clusters within a high−aluminum zeolite, ACS Catal. 12 (2022) 1847–1856.

[31] J. Gu, Z. Zhang, P. Hu, L. Ding, N. Xue, L. Peng, X. Guo, M. Lin, W. Ding, Platinum nanoparticles encapsulated in mfi zeolite crystals by a two-step dry gel conversion method as a highly selective hydrogenation catalyst, ACS Catal. 5 (2015) 6893–6901.

[32] M. Gao, Z. Gong, X. Weng, W. Shang, Y. Chai, W. Dai, G. Wu, N. Guan, L. Li, Methane combustion over palladium catalyst within the confined space of MFI zeolite, Chinese J. Catal. 42 (2021) 1689−1699.

[33] W. Wang, W. Zhou, W. Li, X. Xiong, Y. Wang, K. Cheng, J. Kang, Q. Zhang, Y. Wang, In-situ confinement of ultrasmall palladium nanoparticles in silicalite-1 for methane combustion with excellent activity and hydrothermal stability, Appl. Catal. B-Environ. Energy 276 (2020) 119142.

[34] T. Li, A. Beck, F. Krumeich, L. Artiglia, M.K. Ghosalya, M. Roger, D. Ferri, O. Kröcher, V. Sushkevich, O.V. Safonova, J.A. van Bokhoven, Stable palladium oxide clusters encapsulated in silicalite-1 for complete methane oxidation, ACS Catal. 11 (2021) 7371–7382.

[35] Y. Ma, S. Song, C. Liu, L. Liu, L. Zhang, Y. Zhao, X. Wang, H. Xu, Y. Guan, J. Jiang, W. Song, Y. Han, J. Zhang, P. Wu, Germanium-enriched double-four-membered-ring units inducing zeolite-confined subnanometric Pt clusters for efficient propane dehydrogenation, Nat. Catal. 6 (2023) 506–518.

[36] L. Liu, N. Wang, C. Zhu, X. Liu, Y. Zhu, P. Guo, L. Alfilfil, X. Dong, D. Zhang, Y. Han, Direct imaging of atomically dispersed molybdenum that enables location of aluminum in the framework of zeolite ZSM-5, Angew. Chem. Int. Ed. 59 (2020) 819–825.

[37] X. Tang, J. Ye, L. Guo, T. Pu, L. Cheng, X.M. Cao, Y. Guo, L. Wang, Y. Guo, W. Zhan, S. Dai, Atomic insights into the Cu species supported on zeolite for direct oxidation of methane to methanol via low-damage HAADF-STEM, Adv. Mater. 35 (2023) e2208504.

[38] Y. Lou, J. Ma, W. Hu, Q. Dai, L. Wang, W. Zhan, Y. Guo, X.-M. Cao, Y. Guo, P. Hu, G. Lu, Low-temperature methane combustion over Pd/H-ZSM-5: active Pd sites with specific electronic properties modulated by acidic Sites of H-ZSM-5, ACS Catal. 6 (2016) 8127–8139.

[39] H. Zhang, W. Zhou, X.F. Lu, T. Chen, X.W. Lou, Implanting isolated Ru atoms into edge-rich carbon matrix for efficient electrocatalytic hydrogen evolution, Adv. Energy Mater. 10 (2020) 2000882.

[40] X. Li, P. Shen, X. Li, D. Ma, K. Chu, Sub-nm RuOx Clusters on Pd metallene for synergistically enhanced nitrate electroreduction to ammonia, ACS Nano 17 (2023) 1081–1090.

[41] J.-Z. Qiu, J. Hu, J. Lan, L.-F. Wang, G. Fu, R. Xiao, B. Ge, J. Jiang, Pure siliceous zeolite−supported Ru single−atom active sites for ammonia synthesis, Chem. Mater. 31 (2019) 9413–9421.

[42] X. Chen, Y. Guo, X. Du, Y. Zeng, J. Chu, C. Gong, J. Huang, C. Fan, X. Wang, J. Xiong, Atomic structure modification for electrochemical nitrogen reduction to ammonia, Adv. Energy Mater. 10 (2019) 1903172.

[43] W. Chen, W. Wei, F. Li, Y. Wang, M. Liu, S. Dong, J. Cui, Y. Zhang, R. Wang, K. Ostrikov, S.Q. Zang, Tunable built-in electric field in ru nanoclusters-based electrocatalyst boosts water splitting and simulated seawater electrolysis, Adv. Funct. Mater. (2023) 2310690.

[44] K. Xu, Y. Chen, H. Yang, Y. Gan, L. Wu, L. Tan, Y. Dai, Y. Tang, Partial hydrogenation of anisole to cyclohexanone in water medium catalyzed by atomically dispersed Pd anchored in the micropores of zeolite, Appl. Catal. B-Environ. Energy 341 (2024) 123244.

[45] Y. Li, U. Kanbur, J. Cui, G. Wang, T. Kobayashi, A.D. Sadow, L. Qi, Supported lanthanum borohydride catalyzes CH borylation inside zeolite micropores, Angew. Chem. Int. Ed.. 61 (2022) e202117394.

[46] F. Han, H. Sun, Z. Zhao, Y. Xu, H. Dong, W. Liu, L. Sun, Z. Wang, G. Hou, M. Kitano, W. Li, M. Shen, H. Chen, Selective catalytic reduction of NOx by methanol on metal−free zeolite with brønsted and lewis acid pair, ACS Catal. 12 (2022) 2403–2414.

[47] Q. Ying, Y. Liu, N. Wang, Y. Zhang, Z. Wu, The superior performance of dichloromethane oxidation over Ru doped sulfated TiO_2 catalysts: synergistic effects of Ru dispersion and acidity, Appl. Surf. Sci. 515 (2020) 145971.

[48] Yun Su, Kaixuan Fu, Yanfei Zheng, Na Ji, Chunfeng Song, Degang Ma, Xuebin Lu, Rui Han, Q. Liu, Catalytic oxidation of dichloromethane over Pt−Co/HZSM−5 catalyst: synergistic effect of single−atom Pt, Co3O4, and HZSM−5, Appl. Catal. B-Environ. Energy 288 (2021) 119980.

[49] X. Yu, J. Deng, Y. Liu, L. Jing, R. Gao, Z. Hou, Z. Zhang, H. Dai, Enhanced water resistance and catalytic performance of Ru/TiO_2 by regulating bronsted acid and oxygen vacancy for the oxidative removal of 1,2-dichloroethane and toluene, Environ. Sci. Technol. 56 (2022) 11739–11749.

[50] Q. Ying, Y. Liu, H. Li, Y. Zhang, Z. Wu, A comparative study of the dichloromethane catalytic combustion over ruthenium−based catalysts: Unveiling the roles of acid types in dissociative adsorption and by−products formation, J. Colloid Interface Sci. 605 (2022) 537–546.

[51] F. Lin, Z. Zhang, N. Li, B. Yan, C. He, Z. Hao, G. Chen, How to achieve complete elimination of Cl−VOCs: a critical review on byproducts formation and inhibition strategies during catalytic oxidation, Chem. Eng. J. 404 (2021) 126534.

[52] Q. Dai, Z. Zhang, J. Yan, J. Wu, G. Johnson, W. Sun, X. Wang, S. Zhang, W. Zhan, Phosphate-functionalized CeO_2 nanosheets for efficient catalytic oxidation of dichloromethane, Environ. Sci. Technol. 52 (2018) 13430–13437.

[53] X. Weng, P. Sun, Y. Long, Q. Meng, Z. Wu, Catalytic oxidation of chlorobenzene over $Mn_xCe_{1-x}O_2$/HZSM-5 Catalysts: a study with practical implications, Environ. Sci. Technol. 51 (2017) 8057–8066.

[54] H. Liu, J. Yang, Y. Jia, Z. Wang, M. Jiang, K. Shen, H. Zhao, Y. Guo, Y. Guo, L. Wang, S. Dai, W. Zhan, Significant improvement of catalytic performance for chlorinated volatile organic compound oxidation over RuOx supported on acid−etched Co_3O_4, Environ. Sci. Technol. 55 (2021) 10734–10743.

[55] T. Omotoso, S. Boonyasuwat, S.P. Crossley, Understanding the role of TiO_2 crystal structure on the enhanced activity and stability of Ru/TiO_2 catalysts for the conversion of lignin-derived oxygenates, Green Chem. 16 (2014) 645–652.

[56] J. He, Z. Wu, Q. Gu, Y. Liu, S. Chu, S. Chen, Y. Zhang, B. Yang, T. Chen, A. Wang, B. M. Weckhuysen, T. Zhang, W. Luo, Zeolite-tailored active site proximity for the efficient production of pentanoic biofuels, Angew. Chem. Int. Ed. 60 (2021) 23713–23721.

[57] S. Cao, H. Wang, F. Yu, M. Shi, S. Chen, X. Weng, Y. Liu, Z. Wu, Catalyst performance and mechanism of catalytic combustion of dichloromethane (CH_2Cl_2) over Ce doped TiO_2, J. Coll. Interf. Sci. 463 (2016) 233–241.

[58] I. Maupin, L. Pinard, J. Mijoin, P. Magnoux, Bifunctional mechanism of dichloromethane oxidation over Pt/Al_2O_3: CH_2Cl_2 disproportionation over alumina and oxidation over platinum, J. Catal. 291 (2012) 104–109.

[59] L. Wang, G. Li, P. Wu, K. Shen, Y. Zhang, S. Zhang, R. Xiao, Promoting effect of Pd modification on the M/TiO_2 (M = V, Ce, Mn) catalyst for catalytic oxidation of dichloromethane (DCM), Chem. Eng. Sci. 234 (2021) 116405.

[60] Y. Wang, P. Wang, X. Lu, N. Hu, Q. Wang, S. Wu, W. Deng, L. Wang, Construction of mesoporous Ru@ZSM−5 catalyst for dichloromethane degradation: synergy between acidic sites and redox centres, Fuel 346 (2023) 128337.

[61] S. Xu, Y.−K. Ma, K.−F. Zhang, A.−P. Jia, J. Chen, M.−F. Luo, Y. Wang, J.−Q. Lu, Catalytic oxidation of dichloromethane over phosphate-modified Co_3O_4: Improved performance and control of byproduct selectivity by Co_3O_4 defects and surface acidity, Appl. Surf. Sci. 606 (2022) 154924.

[62] Y. Wang, A.-P. Jia, M.-F. Luo, J.-Q. Lu, Highly active spinel type $CoCr_2O_4$ catalysts for dichloromethane oxidation, Appl. Catal. B-Environ. Energy 165 (2015) 477–486.

[63] G.Y. Popova, T.V. Andrushkevich, Y.A. Chesalov, E.S. Stoyanov, In situ FTIR study of the adsorption of formaldehyde, formic acid, and methyl formiate at the surface of TiO_2 (anatase), Kinet. Catal. 41 (2000) 805–811.

[64] Y. Wang, H.-H. Liu, S.-Y. Wang, M.-F. Luo, J.-Q. Lu, Remarkable enhancement of dichloromethane oxidation over potassium−promoted Pt/Al_2O_3 catalysts, J. Catal. 311 (2014) 314–324.

[65] X. Fei, S. Cao, W. Ouyang, Y. Wen, H. Wang, Z. Wu, A convenient synthesis of core-shell Co_3O_4@ZSM-5 catalysts for the total oxidation of dichloromethane (CH_2Cl_2), Chem. Eng. J. 387 (2020) 123411.

[66] L. Zhang, W. Deng, Y. Cai, Q. Dai, L. Guo, Comparative studies of phosphate−modified CeO_2 and Al_2O_3 for mechanistic understanding of dichloromethane oxidation and chloromethane formation, ACS Catal. 10 (2020) 13109–13124.

[67] C. Ma, D. Wang, W. Xue, B. Dou, H. Wang, Z. Hao, Investigation of formaldehyde oxidation over Co_3O_4-CeO_2 and Au/Co_3O_4-CeO_2 catalysts at room temperature: effective removal and determination of reaction mechanism, Environ. Sci. Technol. 45 (2011) 3628–3634.

[68] Z. Zhang, H. Xia, Q. Dai, X. Wang, Dichloromethane oxidation over $FexZr_{1-x}$ oxide catalysts, Appl. Catal. A-Gen. 557 (2018) 108–118.